Electronic Supplementary Material (ESI) for Physical Chemistry Chemical Physics.
This journal is © the Owner Societies 2020

Supporting Information

Structure of Water and Polymer at the Buried Polymer/Water Interface Unveiled by Heterodyne-Detected Vibrational Sum Frequency Generation

Anton Myalitsin[a,b], Sanat Ghosh[a], Shu-hei Urashima[a,#], Satoshi Nihonyanagi[a,c], Shoichi Yamaguchi[d], Takashi Aoki[e], Tahei Tahara[a,c,*]

Contents

1. Sample Preparation and Characterization

PMMA (Mw ~ 91,000) was purchased from Wako and was dissolved in toluene at the concentration of 10 g/L by stirring overnight. The solution (100 μL) was deposited on the silica substrate (IR grade, Pier Optics, Co. Ltd.) and then spin-coated at 1000 rpm for 30 s. The glass transition temperature (Tg) of the PMMA was 104.8 °C from a thermal analysis of differential scanning calorimetry (DSC, DSC2920, TA Instrument, DE, USA) at heating rates of 20 °C/min. No endothermic peak corresponding to the polymer melting was observed and then the PMMA is amorphous. The substrate was annealed at 160 °C overnight. Thickness of the PMMA film was determined by the ellipsometer. The contact angle with a water droplet was 69°. Ultrapure water (Millipore, 18.2 MΩ cm resistivity) and deuterium oxide (NMR grade, 99.9%, Wako) were used for the water phase in the HD-VSFG experiments.

2. Phase calibration procedure

First, we define the optical configuration of our HD-VSFG measurements as depicted in Figure S1. The media 1, 2 and 3 are SiO_2, PMMA, and water (or air), respectively, with their refractive indices of n_1, n_2 and n_3. The thickness of the medium 2 (d) is either 64 nm or 130 nm. In addition to the three media, the configuration in Figure S1 has two interfaces; the interface between media 1 and 2 (interface I) and that between media 2 and 3 (interface II). Accordingly, the geometry of the HD-VSFG measurement in Figure S1 is considered a five-layer system consisting of the media 1, 2, 3 and interfaces I, II. $\theta_{1,vis/IR}$ and $\theta_{2,vis/IR}$ are the angles of incidence of the visible (vis: ω_1 in the main text) / IR (ω_2) beam in the media 1 and 2, respectively, while $\theta_{1,SF}$ and $\theta_{2,SF}$ are the angles of the sample SF beam in the media 1 and 2. $\theta_{3,SF/vis/IR}$ is the angle of refraction in the medium 3. The incident angles of vis and IR beams at the upper air/silica interface are 38° and 46°, respectively. Beams are refracted at the upper air/silica interface as well as interfaces I and II. These angles in a upper medium (θ_l) and a lower medium (θ_m) are related by the Snell's law,

$$n_l \sin\theta_l = n_m \sin\theta_m \quad . \tag{S1}$$

$\theta_{1,SF}$ is calculated by the momentum conservation parallel to the surface as follows, with ω being frequency:

$$\omega_{SF} n_{1,SF} \sin\theta_{1,SF} = \omega_{vis} n_{1,vis} \sin\theta_{1,vis} + \omega_{IR} n_{1,IR} \sin\theta_{1,IR} \quad . \tag{S2}$$

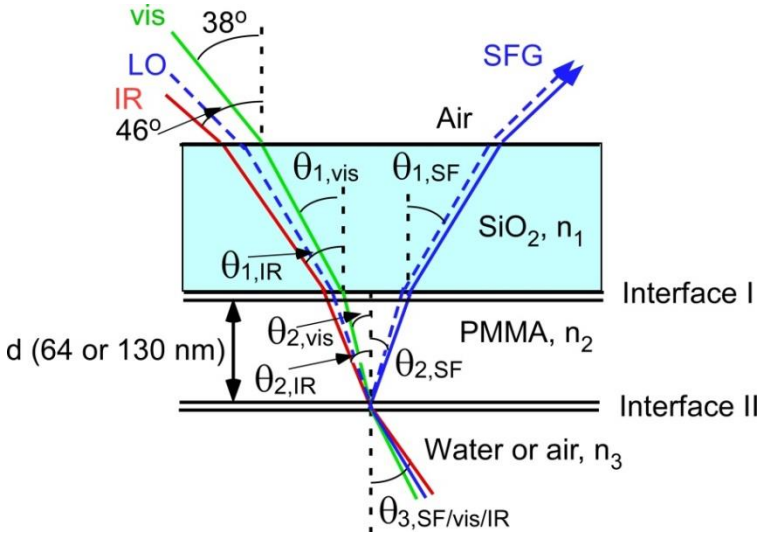

Figure S1. Schematic of the optical geometry of the HD-VSFG measurement of the PMMA thin film interface.

In general, the total intensity of the signal light measured in the HD-VSFG measurement is represented by the sum of sample SF light and local oscillator (LO) reflected at an interface of interest:[1, 2]

$$I = \left|E_{\text{sample}} + \mathrm{r}^{\mathrm{LO}}_{s,sample} E_{\mathrm{LO}} e^{i\omega T}\right|^2$$

$$= \left|E_{\text{sample}}\right|^2 + \left|\mathrm{r}^{\mathrm{LO}}_{s,sample} E_{\mathrm{LO}}\right|^2 + E_{\text{sample}} \mathrm{r}^{*\mathrm{LO}}_{s,sample} E^*_{\mathrm{LO}} e^{i\omega T} + E^*_{\text{sample}} \mathrm{r}^{\mathrm{LO}}_{s,sample} E_{\mathrm{LO}} e^{-i\omega T}\ , \tag{S3}$$

where E_{sample} and E_{LO} are the electric field of the sample SF and the LO, and T is the time delay between the sample SF and the LO (~3 ps), with * representing the complex conjugate. $\mathrm{r}^{\mathrm{LO}}_{s,sample}$ is the coefficient of reflection for the LO beam at the sample interface. The third term in the right hand side of Eq. S3 is picked up using time-domain filtration with Fourier transform to obtain a complex fringe spectrum.[1, 3] For SSP polarization combination used in the present study, the $\chi^{(2)}_{\text{obs}}$ spectrum of a silica/water interface in the OH stretch region can be obtained by normalizing a complex fringe spectrum of the silica/water interface with that of the silica/D_2O-saturated air interface,[4]

$$\chi^{(2)}_{\text{obs}} = \frac{\mathrm{E}_{water} \mathrm{r}^{*\mathrm{LO}}_{s,water} \mathrm{E}^{*}_{LO} \exp(i\omega T)}{\mathrm{E}_{air} \mathrm{r}^{*\mathrm{LO}}_{s,air} \mathrm{E}^{*}_{LO} \exp(i\omega T)} = \frac{\mathrm{r}^{*\mathrm{LO}}_{s,water} F^{water}_{YYZ} \chi^{(2)water}_{YYZ}}{\mathrm{r}^{*\mathrm{LO}}_{s,air} F^{air}_{YYZ} \chi^{(2)air}_{YYZ}}\ , \tag{S4}$$

$$\text{with } F_{YYZ} = L_{Y,SF} L_{Y,vis} L_{Y,IR} \sin\theta_{1,\mathrm{IR}}, \tag{S5}$$

where $\mathrm{L}_{\mathrm{Y,SF}}$ $\mathrm{L}_{\mathrm{Y,vis}}$ $\mathrm{L}_{\mathrm{Z,IR}}$ are the Fresnel factors for the SF, vis, and IR beams, respectively, and $\chi^{(2)}_{YYZ}$ is the relevant tensor element of the second-order susceptibility of the interface. Because $\chi^{(2)air}_{YYZ}$ is electronically and vibrationally non-resonant, it is a real constant. (In fact, it is a positive real constant because $\chi^{(2)}$ of the air/silica interface, which is geometrically opposite to the silica/air interface, is a negative real constant.[4]) $\mathrm{r}^{*\mathrm{LO}}_{s,water} F^{water}_{YYZ} / \mathrm{r}^{*\mathrm{LO}}_{s,air} F^{air}_{YYZ}$ is positive real constant. Thus, this normalization provides $\chi^{(2)}$ of the silica/water interface with the correct phase.

For the thin film polymer sample, we need to consider the contributions of two interfaces (interface I and II). Hence, $\chi^{(2)}_{\text{obs}}$ for the thin film polymer interface is written as,

$$\chi^{(2)}_{obs} = \frac{\mathrm{r}^{*\mathrm{LO}}_{s,water}\left(F^{I,water}_{YYZ} \chi^{(2)I,water}_{YYZ} + F^{II,water}_{YYZ} \chi^{(2)II,water}_{YYZ}\right)}{\mathrm{r}^{*\mathrm{LO}}_{s,air}\left(F^{I,air}_{YYZ} \chi^{(2)I,air}_{YYZ} + F^{II,air}_{YYZ} \chi^{(2)II,air}_{YYZ}\right)}. \tag{S6}$$

The superscript I and II represent the interface I (silica/PMMA) and interface II (PMMA/air or PMMA/water), respectively. Prior experimental and theoretical studies have revealed that nonresonant background in a $\chi^{(2)}$ spectrum of an interface of a dielectric medium arises from the quadrupolar contribution localized at interface.[5, 6] This contribution is originated from the discontinuity of the input or output electric field due to the different refractive indices of two media that consist of the interface. Thus, a larger nonresonant background signal is expected for an interface between two media with a larger difference in refractive indices. As shown in Table S1, the difference in refractive indices between silica and PMMA is very small compared to that between PMMA and air. Therefore, it is reasonable to assume $\chi_{YYZ}^{(2)I,air} \ll \chi_{YYZ}^{(2)II,air}$ for the nonresonant signal measured in air. The verification of this assumption is discussed in the section 4. For the measurement in water, since we are interested in the interfacial water spectrum and the OH resonant $\chi^{(2)}$ is generated only at the interface II, we neglect the contribution from the interface I. In fact, the $\chi^{(2)}$ spectra shown in Figure 2 in the main text is dominated by the OH stretch resonance, hence the neglect of $\chi_{YYZ}^{(2)I,water}$ does not affect our discussion. Then Eq. S6 is simplified as,

$$\chi_{obs}^{(2)} = \frac{r_{s,water}^{*LO}\left(F_{YYZ}^{II,water}\chi_{YYZ}^{(2)II,water}\right)}{r_{s,air}^{*LO}\left(F_{YYZ}^{II,air}\chi_{YYZ}^{(2)II,air}\right)} \quad . \tag{S7}$$

Furthermore, by dividing the $\chi^{(2)}{}_{obs}$ by the relevant Fresnel factors and complex conjugates of coefficients of reflection $\frac{r_{s,water}^{*LO}F_{YYZ}^{II,water}}{r_{s,air}^{*LO}F_{YYZ}^{II,air}}$, we obtain,

$$\chi^{(2)} = \frac{\chi_{YYZ}^{(2)II,water}}{\chi_{YYZ}^{(2)II,air}} \quad . \tag{S8}$$

This is the Fresnel factor and reflectivity corrected $\chi^{(2)}$ spectra which we show in the main text. Because $\chi_{YYZ}^{(2)II,air}$ is vibrationally and electronically nonresonant and hence is pure real, the normalization defined in Eq. S8 can provide $\chi^{(2)}$ spectra of the polymer/water interface with the correct phase. The Fresnel factors and coefficients of reflection used for the correction are given in the next section.

3. Fresnel factor and reflectivity correction

All the spectra shown in the main text have been corrected for the Fresnel factor and reflectivity, which are the linear optical responses of the bulk media. This correction is particularly important when we compare the $\chi^{(2)}$ spectra measured at the PMMA/air and PMMA/water interfaces. In this section, we describe this correction procedure in detail.

The Fresnel factors that take account for the multiple reflections inside the thin film are expressed by the following equations,[7-9]

$$L_{Y,\omega}^{\mathrm{I}} = \frac{t_{12}^{s}}{1+r_{12}^{s}r_{23}^{s}e^{2i\beta}}\left(1 + r_{23}^{s}e^{2i\beta}\right) \ , \tag{S9}$$

$$L_{Z,\omega}^{\mathrm{I}} = \frac{t_{12}^{p}}{1+r_{12}^{p}r_{23}^{p}e^{2i\beta}}\left(1 + r_{23}^{p}e^{2i\beta}\right)\frac{n_1 n_2}{n_{\mathrm{I}}'^{2}}, \tag{S10}$$

$$L_{Y,\omega}^{\mathrm{II}} = \frac{t_{12}^{s}e^{i\Delta}}{1+r_{12}^{s}r_{23}^{s}e^{2i\beta}}\left(1 + r_{23}^{s}\right) \ , \tag{S11}$$

$$L_{Z,\omega}^{\mathrm{II}} = \frac{t_{12}^{p}e^{i\Delta}}{1+r_{12}^{p}r_{23}^{p}e^{2i\beta}}\left(1 + r_{23}^{p}\right)\frac{n_1 n_2}{n_{\mathrm{II}}'^{2}} \ , \tag{S12}$$

where

$$\beta = \frac{2\pi n_2\, d\cos\theta_2}{\lambda} \ , \tag{S13}$$

$$\Delta_{SFG} = \frac{2\pi n_{2,SFG} d}{\lambda_{SFG}\cos\theta_{2,SFG}} \ , \tag{S14}$$

$$\Delta_{vis} = \frac{2\pi n_{2,vis} d}{\lambda_{vis}\cos\theta_{2,vis}} - \frac{2\pi n_{1,vis} d}{\lambda_{vis}}\left(\tan\theta_{2,vis} + \tan\theta_{2,SFG}\right)\sin\theta_{1,vis} \ , \tag{S15}$$

$$\Delta_{IR} = \frac{2\pi n_{2,IR} d}{\lambda_{IR}\cos\theta_{2,IR}} - \frac{2\pi n_{1,IR} d}{\lambda_{IR}}\left(\tan\theta_{2,IR} + \tan\theta_{2,SFG}\right)\sin\theta_{1,IR} \ . \tag{S16}$$

Here, λ denotes the wavelength. r_{lm}^{p} and r_{lm}^{s} are the amplitude ratios of the reflected to incident light in p- and s-polarizations, respectively, at an interface between media *l* and *m* (*lm* = 12 or 23). Similarly, t_{lm}^{p} and t_{lm}^{s} are the amplitude ratios of the transmitted to incident light in p- and s-polarizations, respectively. These are given as follows:

$$t_{lm}^{p} = \frac{2n_l\cos\theta_l}{n_m\cos\theta_l + n_l\cos\theta_m} \ . \tag{S17}$$

$$t_{lm}^{s} = \frac{2n_l\cos\theta_l}{n_l\cos\theta_l + n_m\cos\theta_m} . \tag{S18}$$

$$r_{lm}^{p} = \frac{n_m \cos\theta_l - n_l \cos\theta_m}{n_m \cos\theta_l + n_l \cos\theta_m}. \quad \text{(S19)}$$

$$r_{lm}^{s} = \frac{n_l \cos\theta_l - n_m \cos\theta_m}{n_l \cos\theta_l + n_m \cos\theta_m}. \quad \text{(S20)}$$

n_{I}' and n_{II}', which appear in Eqs. S10 and S12, are the refractive indices of the interfaces I and II, respectively. They were estimated by $n_{\mathrm{I}}' = \sqrt{\frac{n_1^2+n_2^2+4}{2(n_1^{-2}+n_2^{-2}+1)}}$, $n_{\mathrm{II}}' = \sqrt{\frac{n_2^2+n_3^2+4}{2(n_2^{-2}+n_3^{-2}+1)}}$.[10, 11]

The coefficient of reflection considering multiple reflection for LO light is expressed as follows,[12]

$$r_S^{LO} = \frac{r_{12}^s + r_{23}^s e^{-2i\beta}}{1 + r_{12}^s r_{23}^s e^{-2i\beta}} \quad . \quad \text{(S21)}$$

Fresnel factors and the complex conjugate of the reflection coefficients are calculated using the refractive indices shown in Table S1. In this calculation, dispersions of the refractive indices of water and PMMA in the IR region are ignored and only the real parts are taken because it has been shown that the frequency dependences of the Fresnel factors are not significant in the CH and OH stretch regions.[2, 9] The results of the calculation are tabulated in Table S2. With these values, the correction factor for the PMMA/water interface with respect to the air interface $\frac{r_{s,water}^{*\mathrm{LO}} F_{YYZ}^{II,water}}{r_{s,air}^{*\mathrm{LO}} F_{YYZ}^{II,air}}$ is also calculated and shown in Table S2. The $\chi^{(2)}$ spectra without the correction of Fresnel factor and reflectivity are shown in Figures S2 and S3. These uncorrected spectra differ only in the amplitude from the corrected spectra shown in the main text and the spectral shapes are almost unaffected by the correction.

Table S1: The refractive indices of the bulk media used in the calculation.

	n_{silica}[13]	n_{PMMA}[14, 15]	n_{water}[16]	n_{Air}
ω_{SFG} (15519.6 cm^{-1})	1.46	1.49	1.331	1
ω_{vis} (12578.6 cm^{-1})	1.45	1.49	1.329	1
ω_{IR} (3400 cm^{-1})	1.42	1.46	1.283	1

Table S2: Calculated Fresnel factors and reflectivity.

	PMMA/air (d = 64 nm)	PMMA/water (d = 64 nm)	PMMA/air (d = 130 nm)	PMMA/water (d = 130 nm)
F_{YYZ}^{I}	0.62+0.19i	0.51+0.05i	0.42+0.23i	0.46+0.06i
F_{YYZ}^{II}	-0.11+1.02i	-0.06+0.59i	-0.99-0.28i	-0.57-0.16i
r_S^{*LO}	-0.043+0.27i	-0.02+0.07i	-0.27-0.07i	-0.08-0.02i
$\frac{r_{s,water}^{*LO} F_{YYZ}^{II,water}}{r_{s,air}^{*LO} F_{YYZ}^{II,air}}$	N/A	0.15+0.02i	N/A	0.17-0.01i

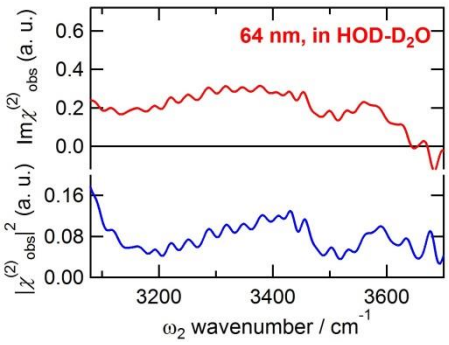

Figure S2. Im$\chi^{(2)}$ spectra of a 64 nm-thick PMMA film/HOD-D_2O interface in the OH stretch region without correction about the Fresnel factor and reflectivity (red line). The corresponding $|\chi^{(2)}|^2$ spectra are also shown in blue.

4. Verification of the phase calibration procedure

In the procedure described above, we assume $\chi_{YYZ,I}^{(2)air} \ll \chi_{YYZ,II}^{(2)air}$. If this is not the case, Eq. S7 is rewritten as

$$\chi_{obs}^{(2)} = \frac{r_{s,water}^{*LO} F_{YYZ}^{II,water} \chi_{YYZ}^{(2)II,water}}{r_{s,air}^{*LO}\left(F_{YYZ}^{I,air}\chi_{YYZ}^{(2)I,air} + F_{YYZ}^{II,air}\chi_{YYZ}^{(2)II,air}\right)} \quad . \tag{S22}$$

In this case, the factor $\frac{r_{s,water}^{*LO} F_{YYZ}^{II,water}}{r_{s,air}^{*LO}\left(F_{YYZ}^{I,air}\chi_{YYZ}^{(2)I,air} + F_{YYZ}^{II,air}\chi_{YYZ}^{(2)II,air}\right)}$ varies with the PMMA film thickness because the complex phase of the Fresnel factors and coefficients of reflections are dependent on the thickness as shown in Table S2. This means that spectra taken with different film thickness would appear differently, if $\chi_{YYZ}^{(2)I,air}$ is significant. Therefore, by comparing the data taken with different film thickness, we can verify the validity of the assumption we made. Figure S3 shows $\chi^{(2)}$ spectra of the silica/PMMA/H_2O interface with the film thickness of 64 nm and 130 nm. The observed Im$\chi^{(2)}$ spectra (red lines) are essentially the same for the two film thicknesses within the experimental error of the present measurements. This indicates that the contribution of $\chi_{YYZ}^{(2)I,air}$ is not significant, verifying the procedure described in the section 2.

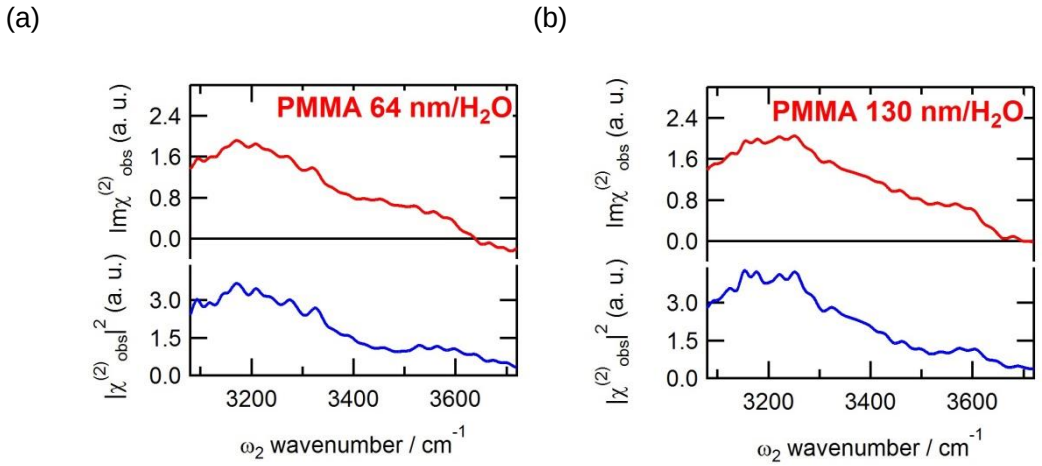

Figure S3. $\chi^{(2)}$ spectra of the PMMA/H_2O interface for the film thickness of (a) 64 nm and (b) 130 nm. The Im$\chi^{(2)}$ spectra and the $|\chi^{(2)}|^2$ spectra are shown in red and blue, respectively. These spectra are not corrected by the Fresnel factor and reflectivity.

5. Contribution of the silica/polymer interface

As discussed in section 2, the $\chi^{(2)}$ signal in the present study can, in principle, be generated not only at the polymer/water or polymer/air interface, but also at the silica/polymer interface. In particular, because the CH moieties are present at both sides of polymer film, the CH band may originate from both interfaces. However, previous homodyne-detected VSFG studies[17,18] concluded that the contribution of the CH stretch vibration of the silica/polymer interface is negligible based on the following observations. First, Tateishi et al. coated a thick PMMA film on a silica prism and

measured VSFG spectra with internal reflection geometry.[17] In this case, because the incident IR light in the CH stretch frequency region is reduced at the polymer/water interface due to the IR absorption by the thick polymer film, the SFG is considered to be predominantly generated at the silica/polymer interface. Their experimental results showed that the CH stretch signal was greatly reduced, compared to the signal observed from a thin polymer film sample. Second, Miyamae and Nozoye measured VSFG spectra of a bulk PMMA substrate with external reflection geometry.[18] In this case, silica/polymer interface was not present. Their experimental results showed that the $\chi^{(2)}$ spectrum of a PMMA substrate is similar to that of a thin film coated on the silica surface. In addition, they observed that the CH bands of the PMMA substrate were significantly suppressed when the PMMA surface was covered with a thin silica film. These observations in the previous studies strongly indicate that the observed CH stretch band predominantly arises from the polymer/air interface.

References

1. S. Yamaguchi and T. Tahara, *J. Chem. Phys.*, 2008, **129**, 101102.
2. S. Urashima, A. Myalitsin, S. Nihonyanagi and T. Tahara, *J. Phys. Chem. Lett.*, 2018, **9**, 4109-4114.
3. S. Nihonyanagi, S. Yamaguchi and T. Tahara, *J. Chem. Phys.*, 2009, **130**, 204704.
4. A. Myalitsin, S. Urashima, S. Nihonyanagi, S. Yamaguchi and T. Tahara, *J. Phys. Chem. C*, 2016, **120**, 9357-9363.
5. S. Yamaguchi, K. Shiratori, A. Morita and T. Tahara, *J. Chem. Phys.*, 2011, **134**, 184705.
6. K. Shiratori and A. Morita, *Bull. Chem. Soc. Jpn.*, 2012, **85**, 1061-1076.
7. Y. Tong, Y. Zhao, N. Li, M. Osawa, P. B. Davies and S. Ye, *J. Chem. Phys.*, 2010, **133**, 034704.
8. E. H. G. Backus, N. Garcia-Araez, M. Bonn and H. J. Bakker, *J. Phys. Chem. C*, 2012, **116**, 23351-23361.
9. L. Wang, S. Nihonyanagi, K. Inoue, K. Nishikawa, A. Morita, S. Ye and T. Tahara, *J. Phys. Chem. C*, 2019, **123**, 15665-15673.
10. X. Zhuang, P. B. Miranda, D. Kim and Y. R. Shen, *Phys. Rev. B*, 1999, **59**, 12632-12640.
11. G. Baranović, *Appl. Spectrosc.*, 2017, **71**, 1039-1049.
12. A. Vasicek, *Optics of thin films*, North-Holand Publishing Company, Amsterdam, 1960.

13. I. H. Malitson, *J. Opt. Soc. Am.*, 1965, **55**, 1205-1209.
14. G. Beadie, M. Brindza, R. A. Flynn, A. Rosenberg and J. S. Shirk, *Appl. Opt.*, 2015, **54**, F139-F143.
15. S. Tsuda, S. Yamaguchi, Y. Kanamori and H. Yugami, *Opt. Express*, 2018, **26**, 6899-6915.
16. G. M. Hale and M. R. Querry, *Appl. Opt.*, 1973, **12**, 555-563.
17. Y. Tateishi, N. Kai, H. Noguchi, K. Uosaki, T. Nagamura and K. Tanaka, *Polym. Chem.*, 2010, **1**, 303-311.
18. T. Miyamae and H. Nozoye, *Surf. Sci.*, 2003, **532-535**, 1045-1050.